# Monitoring of Partially Broken Rotor Bars in Induction Machine Drives

Th.M. Wolbank, G. Stojicic, P. Nussbaumer
Department of Electrical Drives and Machines
Vienna University of Technology
thomas.wolbank@tuwien.ac.at

*Abstract* - **Detection of rotor bar asymmetries in induction machines operated by an inverter can be difficult due to disturbances introduced by the fast switching power devices. Furthermore interference of the fault indicator with control dynamics of the load level lower the accuracy of most detection methods proposed. These disturbances can be avoided if the detection can be realized at standstill of the drive using the inverter as a measurement device. In this paper the sensitivity of a method is analyzed that enables the detection of rotor bar defects at zero load and around standstill. The method is based on the excitation of the machine with voltage pulses generated by the switching of the inverter. Measuring the resulting response of the machine phase currents, the spatial distribution of the transient inductance can be identified with high accuracy. An asymmetry in the rotor bars leads to a distinct change in the spatial distribution of the transient flux linkage and thus also of the transient inductance. The accuracy is such that even partial broken bars can be detected. Measurements on a machine with a specially manufactured copper rotor cage are presented. The resistance of a single bar is stepwise increased by changing the material of the bar from copper to aluminum, brass, and finally steel. It is shown that even the stepwise increase of a single bar resistance before the bar is broken can be clearly detected. It is thus possible to monitor the machine even for a developing rotor defect.**

## I. INTRODUCTION

Inverter fed variable speed drives can already be considered standard in the low and medium power range of modern industrial drive applications. Their dynamic performance is high due to advanced field oriented control concepts.

This dynamic operation in combination with the fast switching power devices leads to additional stress on almost all components of the machine and at the same time demands on reliability are continuously increased.

When looking at fault statistics the breakdown of a drive is caused in about 20% to 30% by defects in the rotor cage [1]-[2]. Rotor cage nowadays is more and more constructed using copper and while the copper bars of medium and high power machines are generally brazed, die cast technique is applied in low power machines to meet efficiency requirements.

The coefficient of thermal expansion of aluminum and copper is much higher than that of the lamination steel. As a result repetitive thermal cycles lead to high stress on the endring-bar connection. These thermal fatigue cycles over time can develop to a crack and finally to a broken bar [3].

From the customer's point of view, a monitoring system that is able to detect not only an already broken bar but also a developing crack offers the possibility to change from preventive to predictive maintenance and thus to significantly save costs.

The topic of monitoring the machine for rotor defects is not new and many attempts have been made in the past years to detect bar defects [4].

Most of the methods published are designed for mains fed machines. For these operating conditions side bands in the stator current are the dominant fault indicators and the methodology is also denoted current signature analysis (CSA) in literature. The means of extracting the fault indicator signal is usually spectrum analysis methods such as different types of Fourier [5]-[6] or wavelet transform [7]-[8], but also pattern recognition techniques [9], or neural network approaches [10], [11]. As these side bands are also influenced by the load level, this effect is addressed using genetic algorithm in [12].

Methods based on CSA are well suited for detecting rotor bar defects in mains fed operation under changing load levels. When the machine is fed by an inverter, detection is usually limited to steady state operation of stator frequency and load. The transients introduced by the PWM scheme and the different control loops then make an accurate estimation of both fundamental frequency and sidebands challenging.

Torque pulsations introduced by the fault are detected in [4] by measuring the stator current spectrum. Wiegner distribution is applied to enable operation at changing stator frequency (10Hz/sec) [13]. In [14], [15] the phasor of the stator current is considered and transferred to the d-q reference frame where the modulus of the phasor is independent of the machine's fundamental wave frequency. The two slip-related side bands introduced by a bar defect then are no longer masked by the fundamental wave.

Using fundamental wave models of the machine to extract a fault indicator is done in [16] where a comparison is made of the torque calculated by the stator and the rotor equation and the resulting data is clustered along the rotor angle. The virtual current of a fundamental wave model is used in [17] to detect rotor defects.

All of the above mentioned methods are based on the interaction of the defect bar with the machine's fundamental wave. They thus require a minimum load level of around 30%-40% in order to detect rotor asymmetries.

Methods able to work at zero load are presented in [18]-[21]. The rotor time constant is identified in different spatial directions in [18]. A pulsating or rotating signal is injected

978-1-4244-5226-2/10/$26.00 ©2010 IEEE

into the machine at standstill in [19]-[21] and the impedance or current ripple is calculated.

Another rotor fault detection method at standstill, however with loaded machine is presented in [22]. There a rotating voltage phasor is injected with low magnitude to reduce the torque. The harmonic spectrum of the resulting current is analyzed and compared to the healthy machine's spectrum. A disadvantage of this approach is that the rotor has to be locked to prevent the machine from starting.

For all of the above mentioned publications no discussion on the possibility to even detect partially broken rotor bars exists.

The method analyzed in the following investigation is based on the injection of voltage pulses generated by the switching of the inverter and measuring the current response.

When applying voltage pulses to the terminals of a machine, using the different output states of a voltage source inverter the resulting current change will be dominated by the transient leakage inductance.

A defective bar leads to a distinct change in the spatial distribution of the transient flux linkage. As a result the transient leakage inductance is modulated depending on the position of the defective bar with respect to the axis of excitation. The proposed method is able to even detect a resistance increase in a single bar what makes it possible to identify partially broken bars at zero load and around standstill.

## II. ONLINE ESTIMATION OF THE TRANSIENT LEAKAGE INDUCTANCE

In the following, the structure and signal processing necessary to carry out the measurements is explained. A more detailed description is given in [23].

The standard way of identifying the dynamic parameters of a system is to observe the step response. In case of an electrical machine the step excitation can be easily realized using the dc link of the voltage source inverter. When changing the inverter output state from inactive to any active switching state a step is applied to the machine terminals with a magnitude equal to the dc link voltage. The system reaction can be detected using the built-in current sensors of the inverter measuring the response of the different phases.

Assuming an ideal symmetrical machine the step response can be calculated using the stator equation of the machine (1).

$$\underline{v}_S = r_S \cdot \underline{i}_S + l_l \cdot \frac{d\underline{i}_S}{d\tau} + \frac{d\underline{\lambda}_R}{d\tau} \qquad (1)$$

The three voltage drops influencing the current reaction of the machine are influenced by the parameters stator resistance $r_S$, leakage inductance $l_l$, and the back emf (time derivative of the rotor flux $\underline{\lambda}_R$).

In the first transient reaction to the voltage step (some ten μs) the dominant voltage drop will be the transient leakage times the time derivative of the current and eventually the back emf (if the machine is running at high speed). An accurate identification of the transient leakage inductance is thus only possible after eliminating the possible influence of the back emf.

This elimination can be realized by evaluating the step responses of two voltage steps with different inverter output states. If these two output states are subsequent the fundamental wave point of operation and especially the direction and magnitude of the back emf will not change significantly. In addition the dc link voltage can be considered constant during the short time period of the pulses.

If the voltage pulses and the sampled current reaction of the two inverter output states are denoted with the indexes I and II the following equations are obtained.

The fundamental wave point of operation of the stator current $\underline{i}_S$ as well as its time derivative can be directly measured. The back emf does not change significantly between the two subsequent pulse excitations thus its influence is eliminated by simply subtracting the two equations in (2). The same applies for the influence of the stator resistance.

$$\begin{aligned} \underline{v}_{S,I} &= r_S \cdot \underline{i}_{S,I} + l_l \cdot \frac{d\underline{i}_{S,I}}{d\tau} + \frac{d\underline{\lambda}_{R,I}}{d\tau} \\ \underline{v}_{S,II} &= r_S \cdot \underline{i}_{S,II} + l_l \cdot \frac{d\underline{i}_{S,II}}{d\tau} + \frac{d\underline{\lambda}_{R,II}}{d\tau} \end{aligned} \qquad (2)$$

Up to now an ideal symmetrical machine has been assumed with the leakage inductance $l_l$ equal the transient inductance according to (1).

As the transient inductance of the machine differs from the fundamental wave leakage it is denoted $l_{l,t}$ in the following.

$$\underline{v}_{S,I} - \underline{v}_{S,II} = l_{l,t}\left(\frac{d\underline{i}_{S,I}}{d\tau} - \frac{d\underline{i}_{S,II}}{d\tau}\right) \qquad (3)$$

When considering fault conditions in the machine it is obvious that the machine no longer will be symmetrical. Due to the existing asymmetry the parameter of the transient leakage must thus be changed from a scalar value in (3) into a complex one. Now the directions of applied pulse voltage ($\underline{v}_{S,I}$-$\underline{v}_{S,II}$) and the resulting current time derivative (slope) will no longer be the same.

This complex transient leakage inductance $\underline{l}_{l,t}$ is composed of a scalar mean or offset value $l_{offset}$ representing the symmetrical machine and a complex value $\underline{l}_{mod}$ representing the fault induced asymmetry with its magnitude and spatial direction.

$$\underline{l}_{l,t} = l_{offset} + \underline{l}_{\mathrm{mod}}, \quad \underline{l}_{\mathrm{mod}} = l_{\mathrm{mod}} \cdot e^{j2\gamma} \qquad (4)$$

The angle γ of the asymmetry portion gives the spatial position of the maximum inductance within one pole pair. The asymmetry has a period of two with respect to the fundamental wave, which corresponds to the expected modulation of a rotor fault. The influence of a broken rotor bar on the transient leakage is repeated for every pole of the stator windings.

When applying a voltage pulse sequence and evaluating the current reaction according to (2),(3) the overall time derivative of the machine current can thus be separated into a 'symmetrical' portion determined by $l_{offset}$ that corresponds to the scalar value $l_{l,t}$ and an 'asymmetrical' portion that is influenced by $\underline{l}_{\mathrm{mod}}$, leading to an angle-dependent cross-coupling.

Separating the value of $\underline{l}_{\mathrm{mod}}$ it is thus possible to determine magnitude and position of the asymmetry what, in case of a rotor bar defect corresponds to the position of the defect bar with respect to the stator windings and the severity of the bar defect (starting from only increased bar resistance of a single bar to one or even more broken bars).

The value of the transient inductance associated to the faultless machine $l_{offset}$ can be identified in advance. Thus for the evaluation algorithm it is sufficient to monitor the resulting current slope of two switching states after elimination of stator resistance and back emf according to (2) and (3).

This leads to (5) where the complex conjugate is marked with $^*$.

$$\begin{aligned}\underline{v}_{S,I} &= l_{offset}\cdot\frac{d\underline{i}_{S,I}}{d\tau}+l_{mod}e^{j2\gamma}\cdot\frac{d\underline{i}^*_{S,I}}{d\tau}\\ \underline{v}_{S,II} &= l_{offset}\cdot\frac{d\underline{i}_{S,II}}{d\tau}+l_{mod}e^{j2\gamma}\cdot\frac{d\underline{i}^*_{S,II}}{d\tau}\end{aligned}\tag{5}$$

The measured current slope of the excitation sequence is thus directly influenced by the magnitude and position of $\underline{l}_{\mathrm{mod}}$ according to (6),

$$\frac{d\underline{i}_{S,I}}{d\tau}-\frac{d\underline{i}_{S,II}}{d\tau}=y_{offset}\cdot\left(\underline{v}_{S,I}-\underline{v}_{S,II}\right)+\underline{y}_{mod}\cdot\left(\underline{v}^*_{S,I}-\underline{v}^*_{S,II}\right)\tag{6}$$

with the values of $y_{offset}$ and $\underline{y}_{mod}$ obtained from inversion as depicted in (7).

$$y_{offset}=\frac{l_{offset}}{l^2_{offset}-l^2_{mod}}\quad \underline{y}_{mod}=-\frac{l_{\mathrm{mod}}}{l^2_{offset}-l^2_{mod}}\cdot e^{j\left(2\gamma-2\arg\left(\underline{v}_{S,I-II}\right)\right)}\tag{7}$$

As can be seen in the previous equations the difference between the two inverter switching states determine the ‘main’ direction of the resulting current change. In symmetrical machines the value of $y_{offset}$ is always clearly dominant with the magnitude of $\underline{y}_{mod}$ even for a faulted machine being only up to 10% of the symmetrical $y_{offset}$.

The excitation, measurement and evaluation structure is shown in Fig. 1 and Fig. 2 for an excitation in phase directions $-W$ ($\underline{v}_{S,I}$) and $+V$ ($\underline{v}_{S,II}$) corresponding to PWM operation in sector 2.

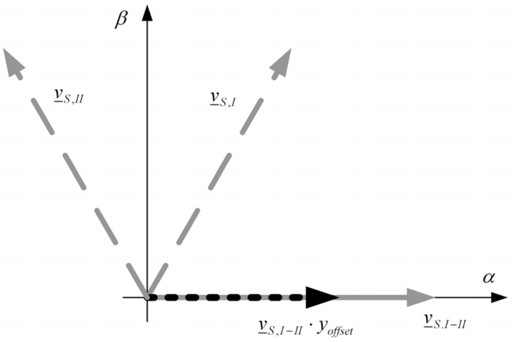


Fig. 1. Influence of $y_{offset}$ (symmetrical machine) on the resulting transient current change for a given pulse sequence ($v_{S,I}$ - $v_{S,II}$= $v_{S,I-II}$ ).

Assuming an ideal symmetrical machine only the inverse inductance $y_{offset}$ influences the time derivative of the current leading to a measured current slope after signal processing (elimination of back emf according to (3)) in the horizontal direction (black dashed phasor).

In Fig. 2 the same resulting excitation direction and the symmetrical current slope are depicted together with an asymmetry caused by a broken bar. The position of the asymmetry is marked by the dashed black phasor denoted “broken bar” pointing in the direction of the maximum inductance. The angle δ(=45°) defines the spatial direction of the maximum transient inductance (broken bar) with respect to the direction of the resulting excitation voltage ($\underline{v}_{S,I-II}$) as indicated.

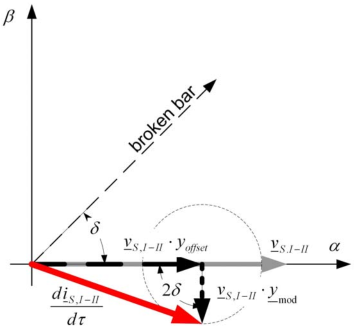


Fig. 2. Influence of $y_{offset}$ and $\underline{y}_{mod}$ on the resulting transient current change for a given pulse sequence ($v_{S,I}$ - $v_{S,II}$= $v_{S,I-II}$ ). Asymmetry position assumed to 45°.

To give a clearer geometrical impression of the influence of the fault induced asymmetry, the value of $\underline{y}_{mod}$ has been clearly increased with respect to $y_{offset}$ in the figure.

As depicted the fault induced asymmetry leads to a current slope (black dotted) orthogonal to the direction of excitation corresponding to twice the angle of the asymmetry (45°).

The resulting current slope after the signal processing is thus the summation of the symmetrical and the fault induced portion. This phasor (red solid) is obtained from the excitation, measurement, and signal processing structure.

The asymmetry depicted (broken bar) is assumed to lead to an ideal sinusoidal distribution of the inductance with a period that equals twice the fundamental wave. If the direction of the asymmetry is the same or opposite as the direction of the resulting excitation voltage (*δ=0°/180°*), the resulting current slope obtained has the same direction as the applied resulting voltage as if the machine was symmetrical.

However, compared to the symmetrical machine its magnitude is either greater or smaller than for the symmetrical case.

The tip of the resulting phasor (red solid) moves along the dotted circle twice when the position of the broken bar (rotor) is changed over one electrical period.

The fault indicator signal can thus be obtained considering the modulation of the resulting current slope phasor with respect to the position of the fault induced asymmetry.

## III. Fault Indicator Measurement and Signal Processing

As was shown in the previous section the resulting current slope resulting from a pulse sequence shows a distinct modulation that contains the information on the machine’s asymmetry. In order to exploit this information for monitoring with high precision it is advantageous to follow some specific signal processing steps.

The excitation is usually generated by a processor that also generates the trigger signals for the measurements. The simplest way for the excitation and the resulting signal processing is to apply a sequence of two active inverter switching states whose voltage phasors point in opposite directions. Thus the excitation axis and the resulting voltage phasor ($\underline{v}_{S,I-II}$) is always parallel with one phase axis.

The measurement of the current's time derivative is realized by taking two current samples during each voltage pulse. It is therefore possible to replace the time derivative $d\underline{i}/d\tau$ by the difference $\Delta\underline{i}_S/\Delta\tau$ between the two samples.

In order to eliminate the back emf, subtraction of the two pulses is done (3). As was already shown in Fig. 2 the resulting current slope obtained contains information of both the symmetrical as well as the asymmetrical portion of the inductance. On a real machine the symmetrical part is responsible for about 90% of the current slope whereas the fault modulation is only around 10%. In addition, the value of the symmetrical inductance also depends on the point of operation. It is thus necessary to clearly separate these two shares in the measured signal.

There are two options to determine or separate the share of the symmetrical inductance in the resulting signal. One is to identify its value in advance on the symmetrical, faultless machine. The parameters to be observed for the identification are the flux as well as the load level of the machine. The second option is to eliminate the symmetrical part using a voltage excitation that sequentially changes its direction in the three phases. Then it is possible to calculate one resulting phasor from three different spatial directions. The share of the symmetrical machine then leads to a zero sequence component that is eliminated.

The resulting phasor thus only contains information on the machine's asymmetry and is also denoted asymmetry phasor. Before it can finally be used as fault indicator it is necessary to apply some further signal processing.

The reason is that the asymmetry induced by the broken rotor bar is not the only asymmetry present in the machine. In every machine even a symmetrical and faultless one there are always some inherent asymmetries present that are also detectable in the asymmetry phasor. The reasons for these modulations are spatial saturation, slotting, and rotor anisotropy. Their modulations will superpose in the asymmetry phasor making the fault detection process challenging. An identification and separation of these inherent asymmetries however, is possible as each of them has deterministic behavior.

### *A. Inherent Asymmetries of Faultless Induction Machines*

The varying level of saturation along the circumference of the airgap is the reason for the saturation saliency. It shows a modulation with a period equal twice that of the fundamental wave. As the fundamental wave is well known, identification is straightforward. In addition, the magnitude of the saturation saliency depends on the flux and load level of the machine. There is an additional dependence of its angular position with respect to the fundamental wave current phasor.

If necessary, it is possible to identify these dependencies in advance. However, as will be shown, it is also possible to clearly identify and eliminate the saturation influence due to its spectral separation, performing specific measurements.

The slotting saliency is influenced by the openings of the slots of the lamination. The rotor slot number determines the period of this modulation. The point of operation has almost negligible influence.

Depending on the design of the machine there is also an additional component detectable that arises when both saturation and slotting are present. It is an intermodulation component that together with the saturation component also depends on the point of operation.

Looking at the harmonic content of the asymmetry phasor the inherent asymmetries are clearly visible as is depicted in Fig. 3. The machine has 4 poles and an unskewed rotor with 28 open rotor slots. The figure shows operation at rated flux/zero load. The slotting saliency is easily detectable from the dominating +28$^{th}$ harmonic component together with a smaller -28$^{th}$. This -28$^{th}$ harmonic indicates a slight asymmetry in the slotting modulation (non-sinusoidal spatial distribution of the responsible inductance).

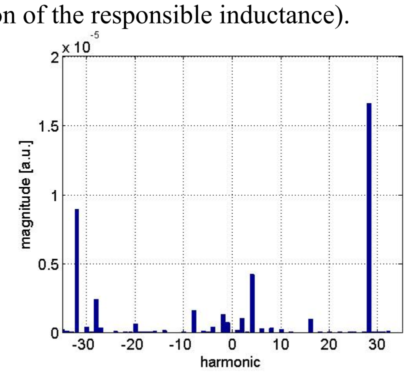


Fig. 3. Harmonic content of the asymmetry phasor of a faultless induction machine at rated flux/zero load (horizontal axis: harmonic order scaled to one mechanical revolution; a.u. arbitrary unit).

The saturation saliency leads to the +4$^{th}$ harmonic. As the machine has two pole pairs and the saturation asymmetry results in a second harmonic with respect to the fundamental wave (only saturation is detected not its direction) the corresponding component is the +4$^{th}$ harmonic depicted in the figure.

Finally there is also a -32$^{nd}$ harmonic resulting from the mentioned intermodulation between saturation and slotting saliency.

### *B. Separation of Inherent Asymmetries*

To develop a fault indicator signal the inherent saliency components have to be removed from the asymmetry phasor. Signal. This can be done very effectively using a spectral filter. However, removing the mentioned harmonic components depicted in Fig. 3 would also eliminate the fault induced component. It is thus necessary to analyze the fault induced saliency before setting up the measurement and separation procedure.

The asymmetry phasor is dominated by the transient inductance. The corresponding flux linkage is slot leakage and zigzag flux. In a symmetrical machine, the rotor cage has a relative long electrical time constant of typically some hundred milliseconds. It is blocking any transient flux changes from the rotor thus limiting the transient flux to the surface outside the cage.

In case of a broken bar the zigzag flux, passing the air gap between stator and rotor to bridge the slot openings of both stator and rotor, can avoid the slot opening or the small slot bridge. It then passes within the lower saturated area (compared to the tooth tips) underneath the broken bar.

The position of this asymmetry in the transient flux linkage is influenced by the mechanical rotor angle. In the case of a machine with four poles as depicted in Fig. 3 this leads to a signal component of the asymmetry phasor with a period of four with respect to the mechanical angle.

The fault induced asymmetry has thus the same harmonic order as the saturation saliency. To obtain a fault indicator signal with high sensitivity to bar defects it is thus necessary to separate the saturation and fault induced asymmetries in a separate step. This separation can be done in three different ways.

- The first option is to operate the machine with zero flux.
- Alternatively it is possible to identify magnitude and angular position of the saturation saliency in advance.
- The third option is to use a special measurement procedure as described in the following.

This third method has been applied in this investigation. Looking at the spectral composition of the asymmetry phasor the $4^{th}$ harmonic caused by the saturation saliency is fixed with twice the angle of the stator current phasor. On the other side the $4^{th}$ harmonic induced by the bar defect is fixed with the rotor angle times the number of poles.

Performing the measurements at zero load and with a fixed flux level a set of measurements can be done each for a different spatial direction of the saturation saliency with respect to the rotor surface.

For each position of the saturation saliency on the rotor surface at least one period of its modulation along the stator is observed. Then a Fourier analysis is done and all saliency harmonics except the interesting one are removed. The measurement and harmonic elimination is then repeated for the next position of the saturation saliency on the rotor until at least one full period of its modulation is reached.

This leads to a set of asymmetry phasors that represent only the bar fault induced saliency, each for a different position of the saturation saliency.

Then another Fourier transform is done using the results of the previous transform of each saturation position with respect to the rotor surface. Eliminating the corresponding modulation leaves the mean- or offset-value that now only corresponds to the bar fault asymmetry.

## IV. Measurement Results and Verification of Detection Sensitivity

The measurements for the sensitivity analysis were performed on a machine with two poles, 36 stator slots and a rotor with 28 unskewed rotor bars. To allow an accurate and reproducible modification of each rotor bar resistance the cage was build up of solid copper bars that can be screwed in/to the two copper end rings. Thus it is possible to remove or replace each single bar for example by a partially broken bar or by a bar made from a different material to allow a fine adjustment of the cage asymmetry.

The setup consisted of this special machine, a voltage source inverter, as well as measurement/control electronics.

The excitation sequence and measurement was done as described in the previous section.

The variation of the bar resistance was done in six steps starting from a symmetrical cage till the removal of a single bar. The first two asymmetry levels are obtained using copper bars that are partially cut. They are denoted bar1 and bar2 in the following and their resulting increase in bar resistance with respect to solid copper was measured to +13% and +38%. The remaining asymmetry levels are obtained using different materials starting with aluminum then brass and finally steel. Table I shows the variations applied and their resistance levels.

TABLE I
Bar Resistances Applied for the Measurements

| | abs. resistance [Ω] | rel. resistance [%] |
|---|---|---|
| copper | $44{,}1\ 10^{-6}$ | 100 |
| bar1 | $50{,}0\ 10^{-6}$ | 113 |
| bar2 | $60{,}8\ 10^{-6}$ | 138 |
| aluminum | $79{,}1\ 10^{-6}$ | 179 |
| brass | $209\ 10^{-6}$ | 474 |
| steel | $380\ 10^{-6}$ | 862 |

The first set of measurements was performed on a symmetrical rotor with all bars well fixed in the cage as a reference. All further measurements are scaled based on this reference.

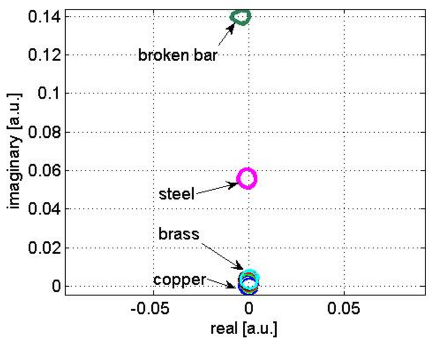

Fig. 4. Locus of the asymmetry phasor as a function of the saturation saliency angle with respect to the rotor surface (a.u. arbitrary unit).

The above Fig. 4 gives an overview of the results before applying the second Fourier transform to eliminate the influence of the saturation saliency.

Each circle represents one rotor bar asymmetry level. The circle is obtained when repeating the measurements for different positions of the saturation on the rotor. As can be seen, the removal of one bar ("broken bar") leads to very distinct change much higher than the modulation caused by the saturation saliency.

The results after elimination of the saturation saliency are given in Fig. 5. This signal represents the final fault indicator.

As can be seen the proposed measurement and signal processing method allow a very accurate monitoring of the rotor bar symmetry. Even a developing fault can thus be clearly identified.

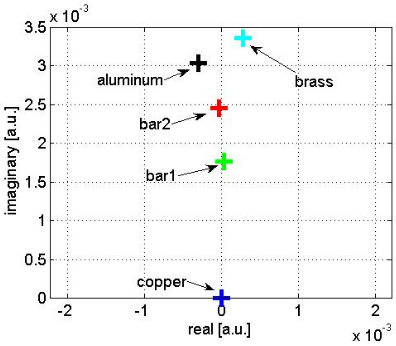


Fig. 5. Value of resulting fault indicator signal depending on rotor bar asymmetry (a.u. arbitrary unit).

To further test the performance of the fault indicator the statistical properties of the signal have been investigated based on 100 measurements of the same saliency positions. The standard deviation for these measurements results to $33 \cdot 10^{-6}$ what is clearly below the noise level regarding all investigated fault conditions.

## V. Conclusions

A new measurement and signal processing setup has been proposed to calculate a fault indicator signal. It is based on an excitation of the machine with voltage pulses and the measurement of the resulting current reaction. It was shown that a rotor bar asymmetry and the inherent saliencies superpose in the resulting asymmetry phasor.

Applying the measurement procedure over one period of each modulation and performing spectral filtering allows a clear separation of both effects. The fault indicator signal obtained after applying the procedure has very high accuracy. It was shown by measurements that even an increase of a single bar resistance of only 13% can be clearly detected. The proposed setup is thus able to already detect a rotor defect in an early stage even before a bar is broken.

## References

[1] A. H. Bonnet and C. Yung, “Increased efficiency versus increased reliability,” IEEE Industry Applications Magazine, vol.14, no.1, pp.29-36, 2008.

[2] IEEE Committee Report, “Report of large motor reliability survey of industrial and commercial installation, Part I and Part II,” IEEE Transactions on Industry Applications, vol.21, no.4, pp.853–872, 1985

[3] M. Hodowanec and W. R. Finley, “Copper versus Aluminum - Which Construction is Best?,” *IEEE Industry Applications Magazine,* vol.8, no.4, pp. 14-25, 2002

[4] A. Bellini, F. Filippetti, C. Tassoni and G. Capolino, “Advances in Diagnostic Techniques for Induction Machines,” IEEE Transactions on Industrial Electronics, vol.55, no.12, pp.4109-4126, 2008

[5] W. Le Roux, R. G. Harley and T. G. Habetler, “Detecting Rotor Faults in Low Power Permanent Magnet Synchronous Machines,” IEEE Transactions on Power Electronics, vol.22, no.1, pp.322-328, 2007

[6] A. Bellini, A. Yazidi, F. Filippetti, C. Rossi and G. Capolino, “High Frequency Resolution Techniques for Rotor Fault Detection of Induction Machines,” IEEE Transactions on Industrial Electronics vol.55, no.2, pp.4200-4209, 2008

[7] S.H. Kia, H. Henao and G. Capolino, “Diagnosis of Broken Bar Fault in Induction Machines Using Discrete Wavelet Transform without Slip Estimation,” IEEE Transactions on Industry Applications, vol.45, no.4, pp.1395-1404, 2009

[8] M. Riera-Guasp, J. A. Antonino-Daviu, M. Pineda-Sanchez, R. Puche-Panadero and J. Perez-Cruz, “A General Approach for the Transient Detection of Slip-Dependent Fault Components Based on the Discrete Wavelet Transform,” IEEE Transactions on Industrial Electronics, vol.55, no.12, pp.4167-4180, 2008

[9] M. Haji and H. A. Toliyat, “Pattern Recognition - a Technique for Induction Machines Rotor Fault Detection eccentricity and Broken Bar Fault,” Proceedings of Industry Applications Annual Conference IAS, vol.3, pp.1572-1578, 2001

[10] B. Ayhan, M.-Y. Chow and M.-H. Song, “Multiple Discriminant Analysis and Neural-Network-Based Monolith and Partition Fault-Detection Schemes for Broken Rotor Bar in Induction Motors,” IEEE Transactions on Industrial Electronics, vol.53, no.4, pp.1298-1308, 2006

[11] F. Filippetti, G. Franceschini and C. Tassoni, “Neural networks aided on-line diagnostics of induction motor rotor faults,” IEEE Transactions on Industry Applications, vol.31, no.4, pp.892-899, 1995

[12] H. Razik, M. B. de Rossiter Corrêa and E. R. C. da Silva, “A Novel Monitoring of Load Level and Broken Bar Fault Severity Applied to Squirrel-Cage Induction Motors Using a Genetic Algorithm,” IEEE Transactions on Industrial Electronics, vol.56, no.11, pp.4615-4626, 2009

[13] M. Blödt, D. Bonacci, J. Regnier, M. Chabert and J. Faucher, “On-Line Monitoring of Mechanical Faults in Variable-Speed Induction Motor Drives Using the Wigner Distribution,” IEEE Transactions on Industrial Electronics, pp.522-531, 2008

[14] S. M. A. Cruz, H. A. Toliyat and A. J. Marques Cardoso, “DSP implementation of the multiple reference frames theory for the diagnosis of stator faults in a DTC induction motor drive,” IEEE Transactions on Energy Conversion, pp.329-335, 2005

[15] S. M. A. Cruz and A. J. Marques Cardoso, “Rotor Cage Fault Diagnosis in Three-Phase Induction Motors, by Extended Park's Vector Approach,” Proceedings of International Conference on Electrical Machines, pp.1844-1848, 1998

[16] C. Kral, F. Pirker, G. Pascoli and H. Kapeller, “Robust Rotor Fault Detection by Means of the Vienna Monitoring Method and a Parameter Tracking Technique,” IEEE Transactions on Industrial Electronics, vol.55, no.12, pp. 4229-4237, 2008

[17] S. M. Cruz, A. Stefani, F. Filippetti and A. J. Marques Cardoso, “A New Model-Based Technique for the Diagnosis of Rotor Faults in RFOC Induction Motor Drives,” IEEE Transactions on Industrial Electronics, vol.55, no.12, pp.4218-4228, 2008

[18] T. Wolbank, J. Machl, R. Schneiderbauer, “Detecting Rotor Faults in Inverter-Fed Induction Machines at Zero Load,” Proceedings of International Power Electronics and Motion Control Conference, EPE-PEMC, Riga, Latvia, pp.1-6, 2004

[19] B. Kim, K. Lee, J. Yang, S. B. Lee, E. Wiedenbrug and M. Shah, “Automated detection of rotor faults for inverter-fed induction machines under standstill conditions,” IEEE Energy Conversion Congress and Exposition, pp.2277-2284, 2009

[20] S. B. Lee, J. Yang, J. Hong, B. Kim, J. Yoo, K. Lee, J. Yun, M. Kim, K. Lee, E. J. Wiedenbrug, and S. Nandi, “A New Strategy for Condition Monitoring of Adjustable Speed Induction Machine Drive Systems,” Proceedings of IEEE International Symposium on Diagnostics for Electric Machines, Power Electronics and Drives, SDEMPED, pp.1-9, 2009

[21] C. Concari, G. Franceschini and C. Tassoni, “Self-commissioning procedures to detect parameters in healthy and faulty induction drives,” Proceedings of IEEE International Symposium on Diagnostics for Electric Machines, Power Electronics and Drives, pp.1-6, 2009

[22] B. Akin, A. B. Ozturk, H. A. Toliyat and M. Rayner, “DSP-Based Sensorless Electric Motor Fault-Diagnosis Tools for Electric and Hybrid Electric Vehicle Powertrain Applications,” IEEE Transactions on Vehicular Technology, vol.58, no.6, 2679-2688, 2009

[23] Wolbank, T.; Nussbaumer, P.; Chen, H. & Macheiner, P., “Non-invasive detection of rotor cage faults in inverter fed induction machines at no load and low speed”, Proceedings of IEEE International Symposium on Diagnostics for Electric Machines, Power Electronics and Drives, SDEMPED, pp.1-7, 2009